Supplementary Information of "Anisotropic Scattering in Radio-Echo Sounding: Insights from Northeast Greenland"

Tamara Annina Gerber[1], David A. Lilien[2,3], Niels F. Nymand[1], Daniel Steinhage[4], Olaf Eisen[4,5], and Dorthe Dahl-Jensen[1,2]

[1]Section for the Physics of Ice, Climate and Earth, Niels Bohr Institute, University of Copenhagen, Copenhagen, Denmark.
[2]Centre for Earth Observation Science, University of Manitoba, Winnipeg, MB, Canada.
[3]Department of Earth and Atmospheric Sciences, Indiana University, Bloomington, IN, USA
[4]Alfred Wegener Institute Helmholtz Centre for Polar and Marine Research, Bremerhaven, Germany
[5]Department of Geosciences, University of Bremen, Bremen, Germany.
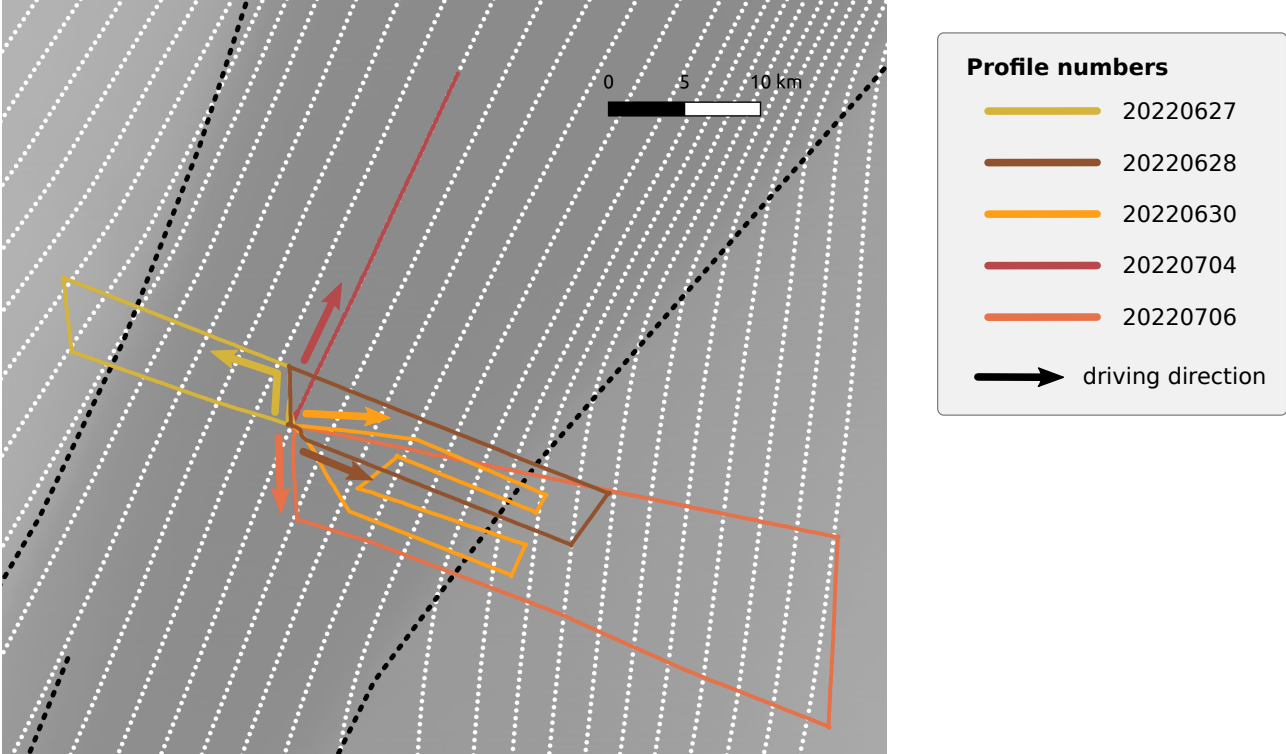
Supplementary Figures

Fig. S1: Overview of profile names and driving directions. Profile '20220704' was measured double on the way back to camp upon turning at the downstream end.
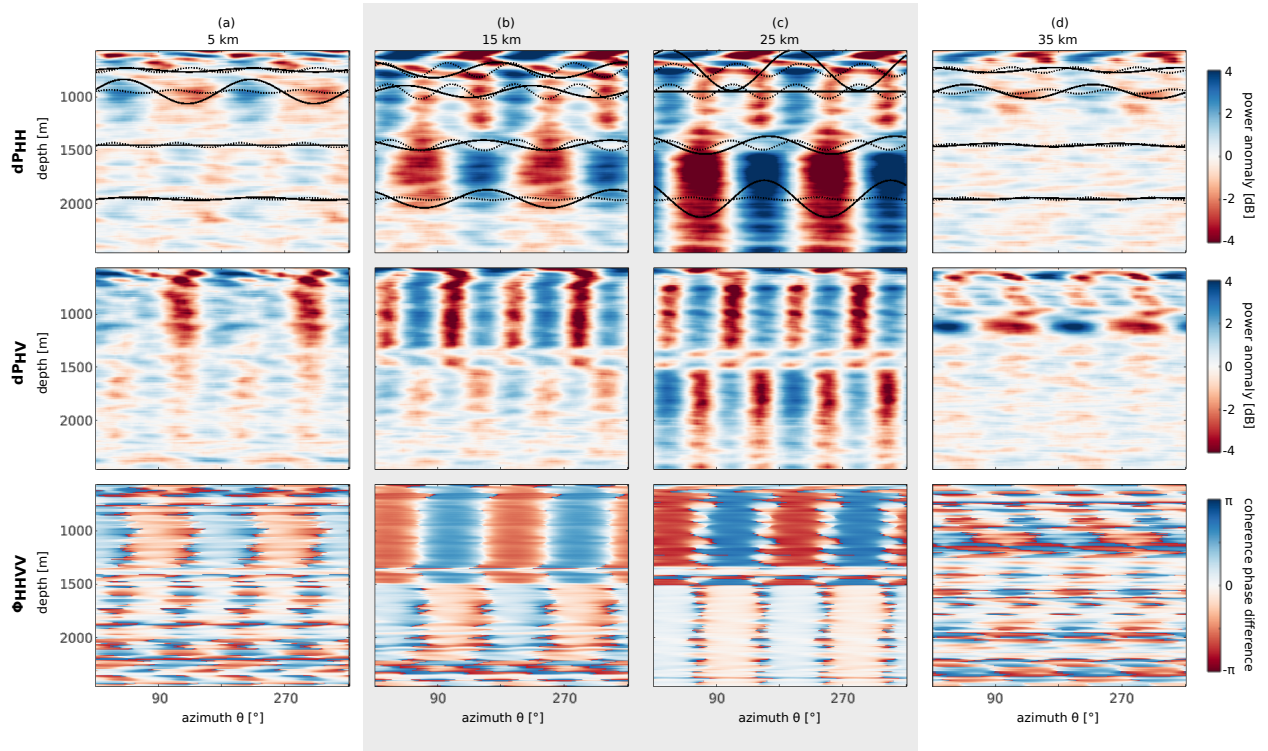
Fig. S2: Synthesized azimuthal radar response for profile '20220627': top panels show the co-polarized power anomaly dP$_{HH}$, middle panels show the cross-polarized power anomaly dP$_{HV}$, and bottom panels show the coherence phase difference ϕ_{HHVV}. White background indicates locations inside the ice stream and light gray is less than 3 km from the shear margin.
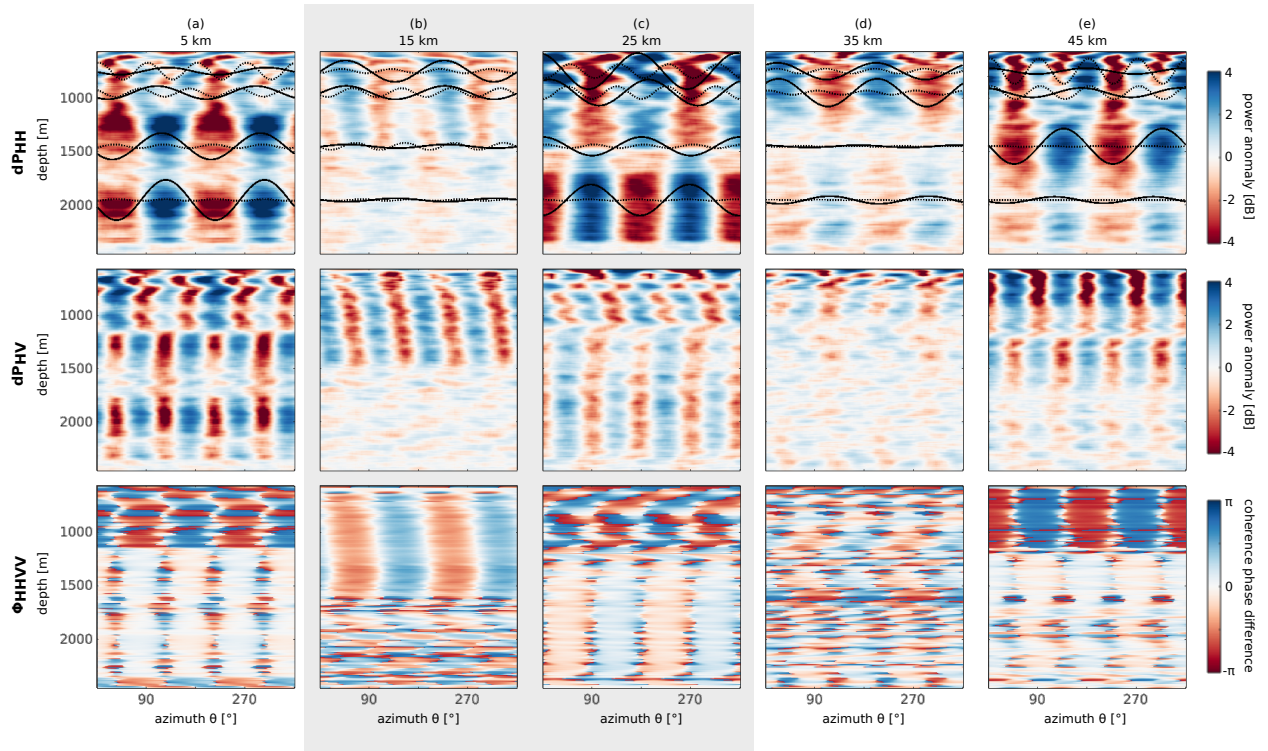

Fig. S3: Synthesized azimuthal radar response for profile '20220628': top panels show the co-polarized power anomaly dP$_{HH}$, middle panels show the cross-polarized power anomaly dP$_{HV}$, and bottom panels show the coherence phase difference ϕ_{HHVV}. White background indicates locations inside the ice stream and light gray is less than 3 km from the shear margin.
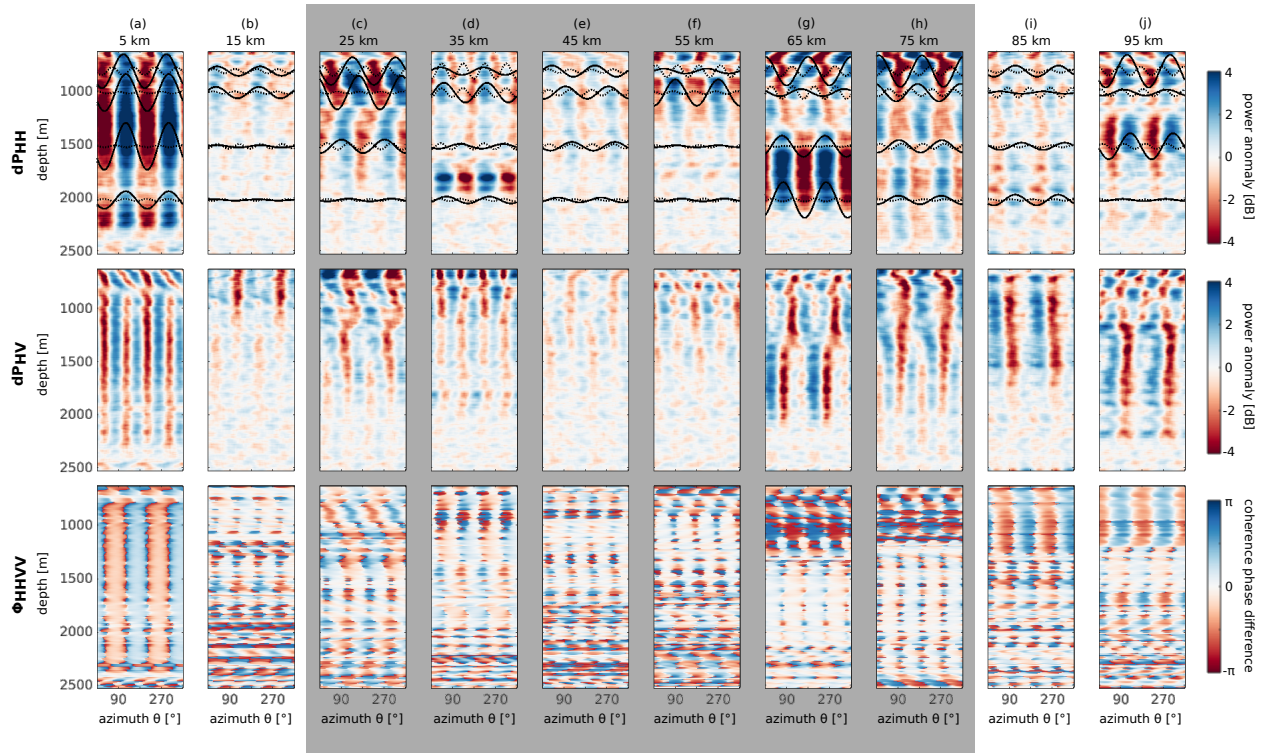
Fig. S4: Synthesized azimuthal radar response for profile '20220628': top panels show the co-polarized power anomaly dP$_{HH}$, middle panels show the cross-polarized power anomaly dP$_{HV}$, and bottom panels show the coherence phase difference ϕ_{HHVV}. White background indicates locations inside the ice stream and dark gray is outside the NEGIS.
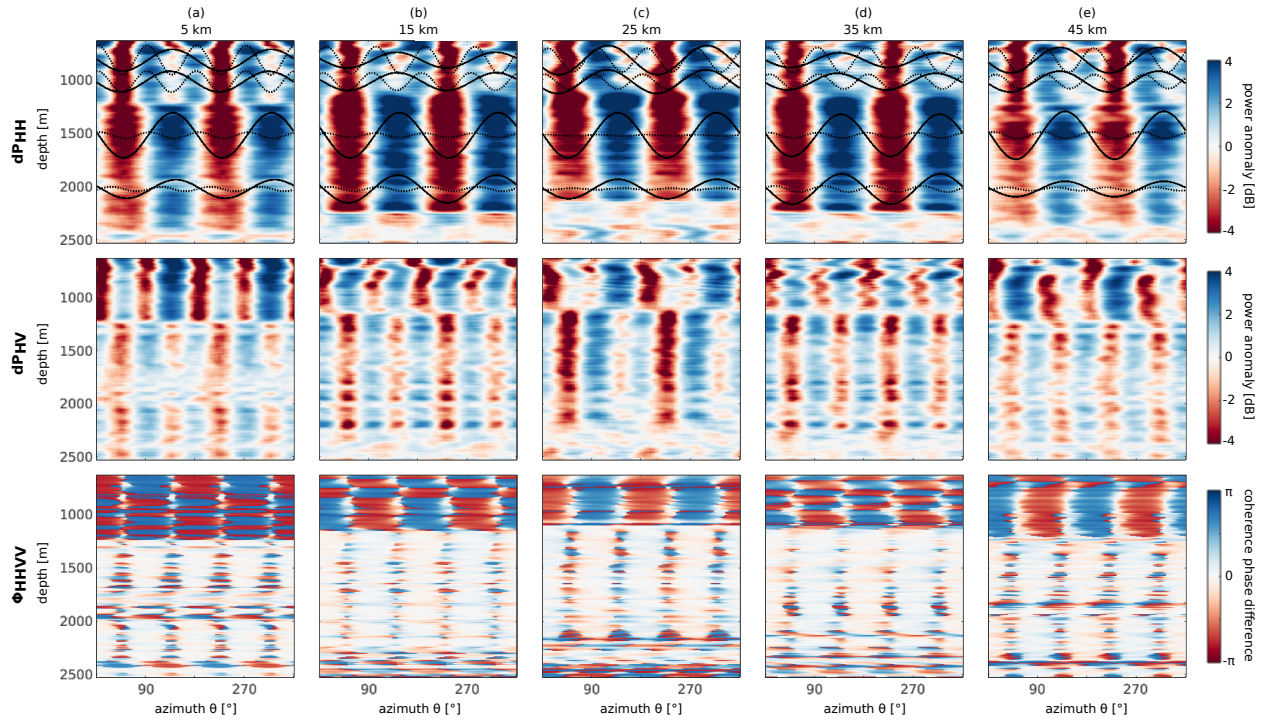

Fig. S5: Synthesized azimuthal radar response for profile '20220704': top panels show the co-polarized power anomaly dP$_{HH}$, middle panels show the cross-polarized power anomaly dP$_{HV}$, and bottom panels show the coherence phase difference ϕ_{HHVV}.
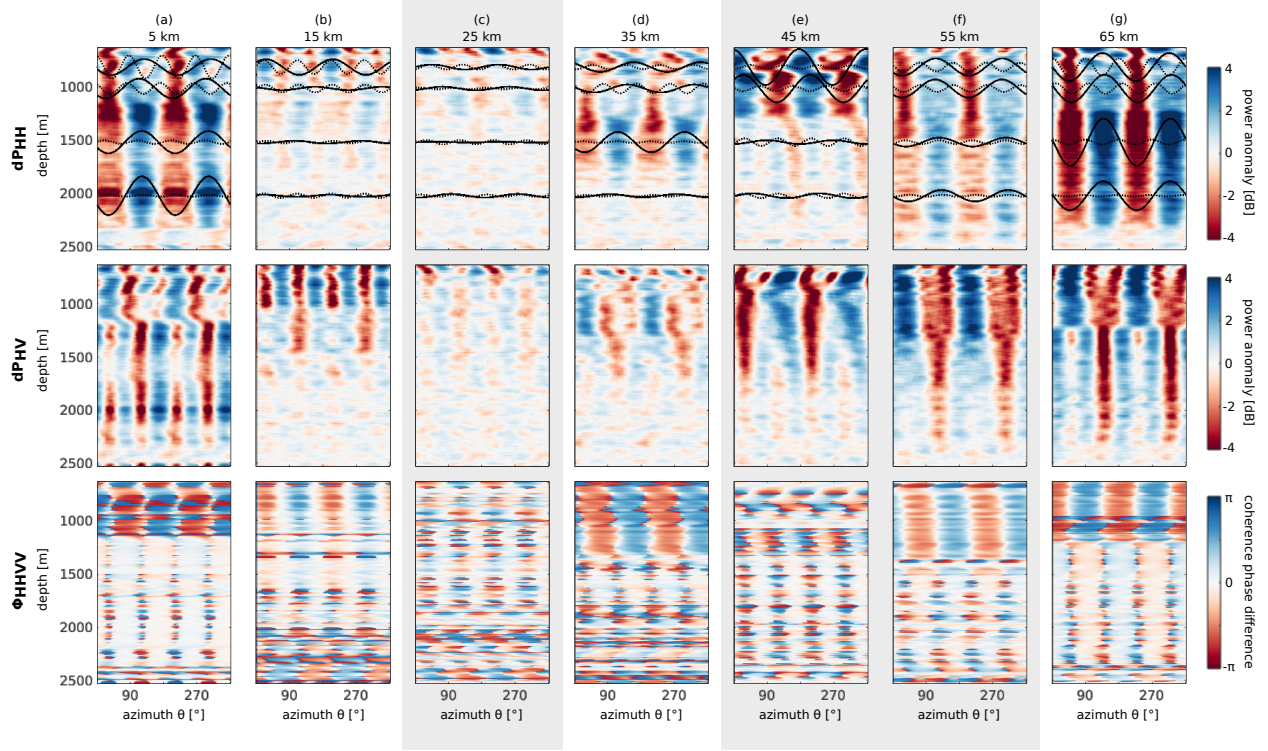
4

Fig. S6: Synthesized azimuthal radar response for profile '20220706': top panels show the co-polarized power anomaly dP_{HH}, middle panels show the cross-polarized power anomaly dP_{HV}, and bottom panels show the coherence phase difference ϕ_{HHVV}. White background indicates locations inside the ice stream, light gray is less than 3 km from a shear margin.
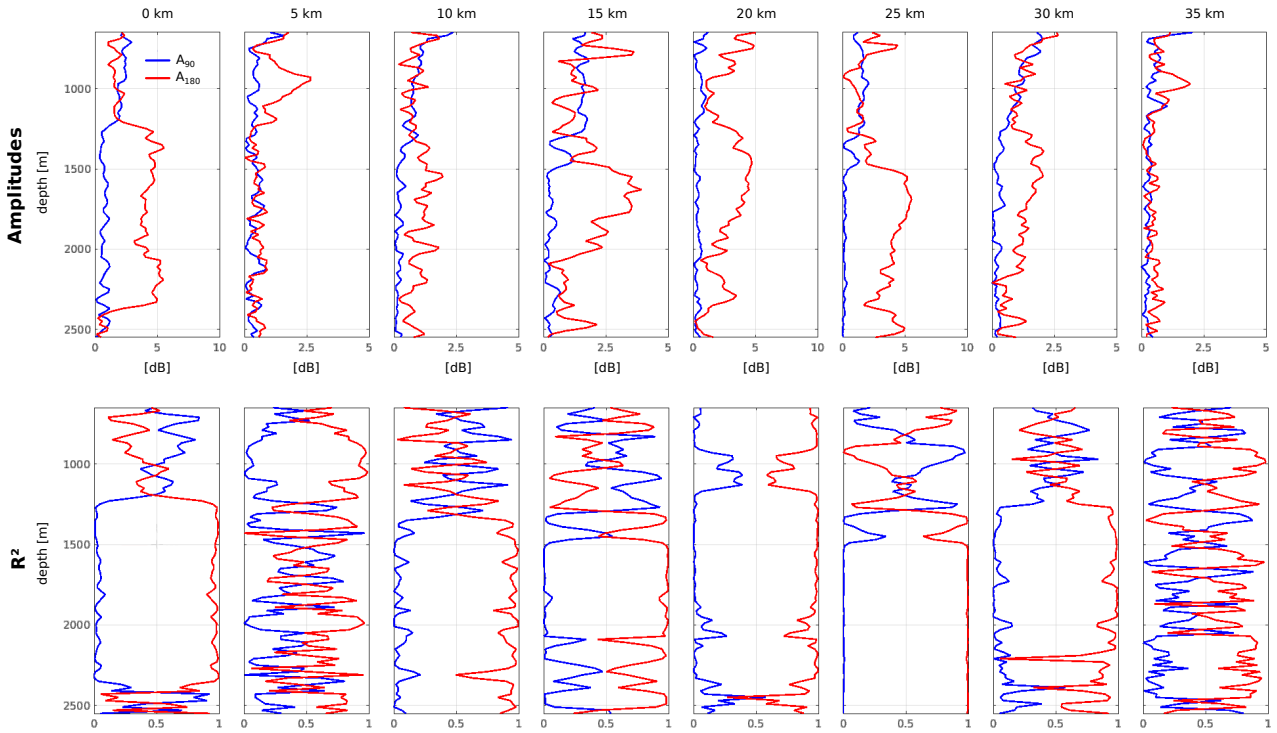

Fig. S7: Amplitudes and goodness of fit for 90°- and 180°-periodic sine curve in profile '20220627'. Top panels show the amplitudes of birefringence (blue) and scattering (red) in dB at 5 km intervals along the profile, with start and driving direction indicated in Fig. S1. Bottom panels show the coefficient of determination (R^2), indicating the goodness of the fit, ranging from 0 to 1, for both curves.
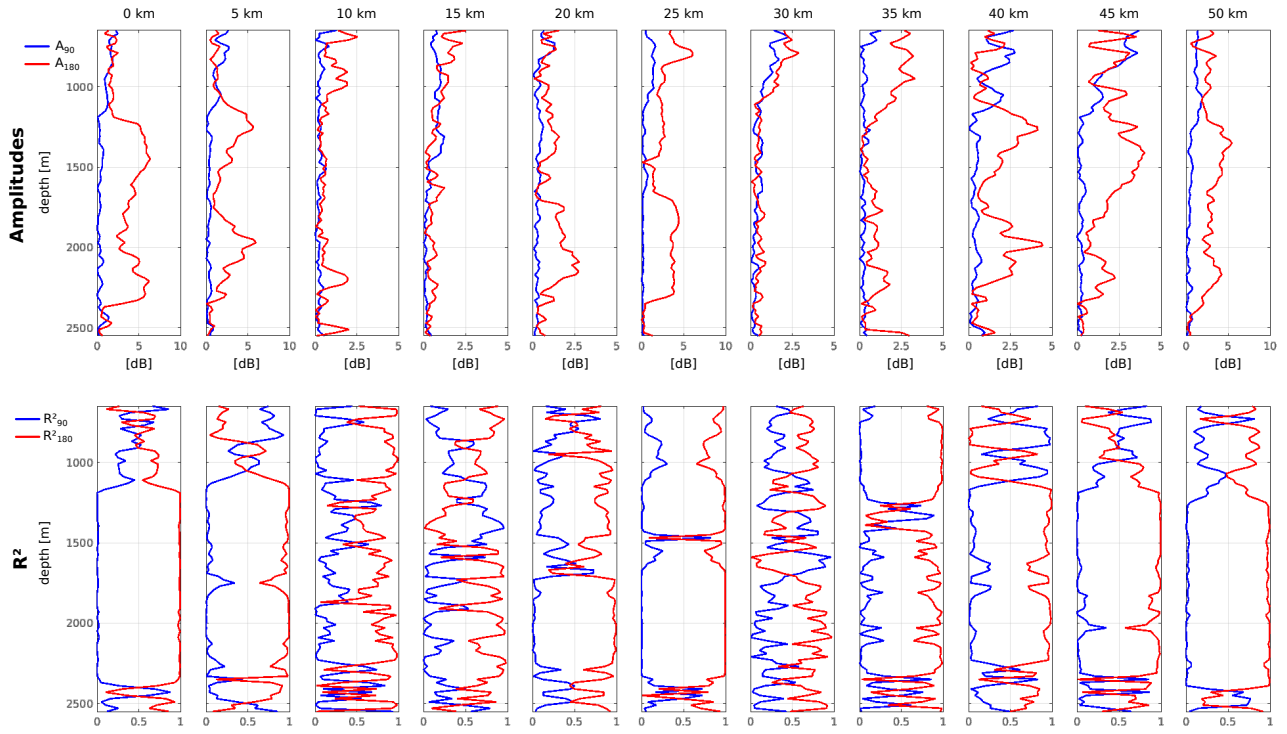
Fig. S8: Amplitudes and goodness of fit for 90°- and 180°-periodic sine curve in profile '20220628'. Top panels show the amplitudes of birefringence (blue) and scattering (red) in dB at 5 km intervals along the profile, with start and driving direction indicated in Fig. S1. Bottom panels show the coefficient of determination (R^2), indicating the goodness of the fit, ranging from 0 to 1, for both curves.
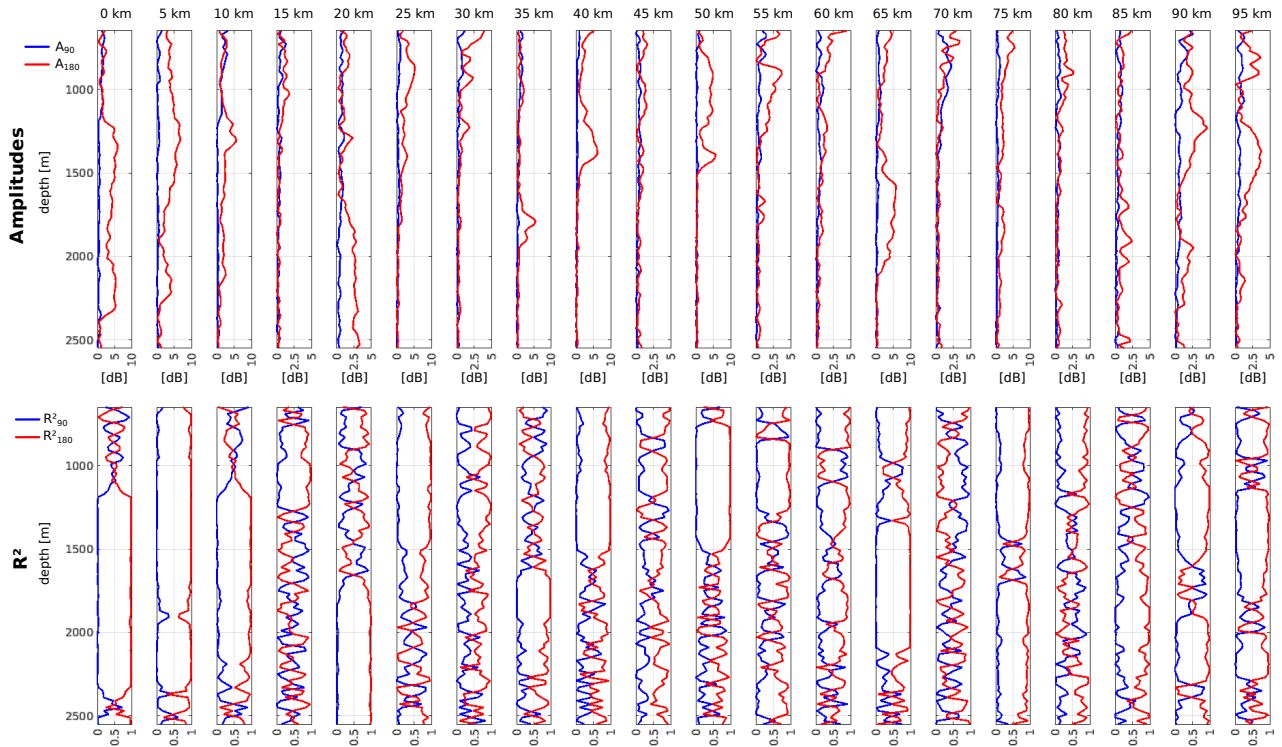

Fig. S9: Amplitudes and goodness of fit for 90°- and 180°-periodic sine curve in profile '20220630'. Top panels show the amplitudes of birefringence (blue) and scattering (red) in dB at 5 km intervals along the profile, with start and driving direction indicated in Fig. S1. Bottom panels show the coefficient of determination (R^2), indicating the goodness of the fit, ranging from 0 to 1, for both curves.
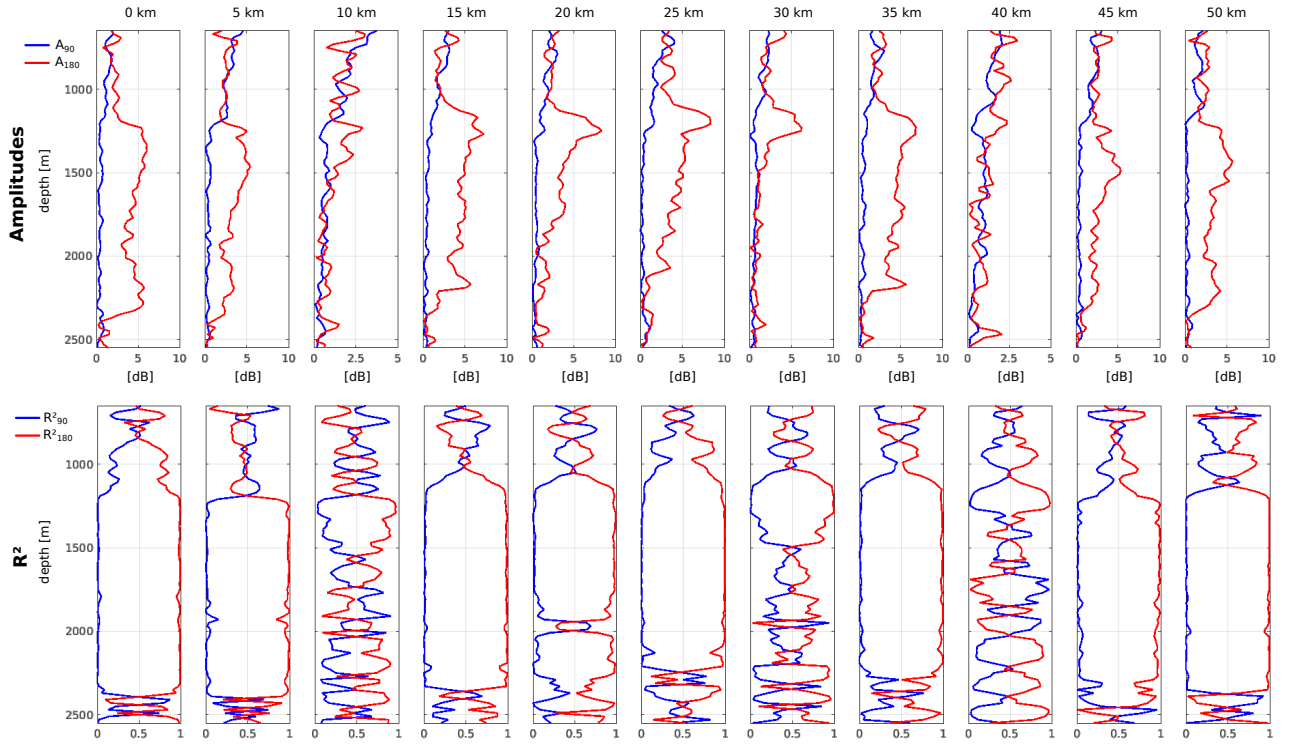
Fig. S10: Amplitudes and goodness of fit for 90°- and 180°-periodic sine curve in profile '20220704'. Top panels show the amplitudes of birefringence (blue) and scattering (red) in dB at 5 km intervals along the profile, with start and driving direction indicated in Fig. S1. Bottom panels show the coefficient of determination (R^2), indicating the goodness of the fit, ranging from 0 to 1, for both curves.
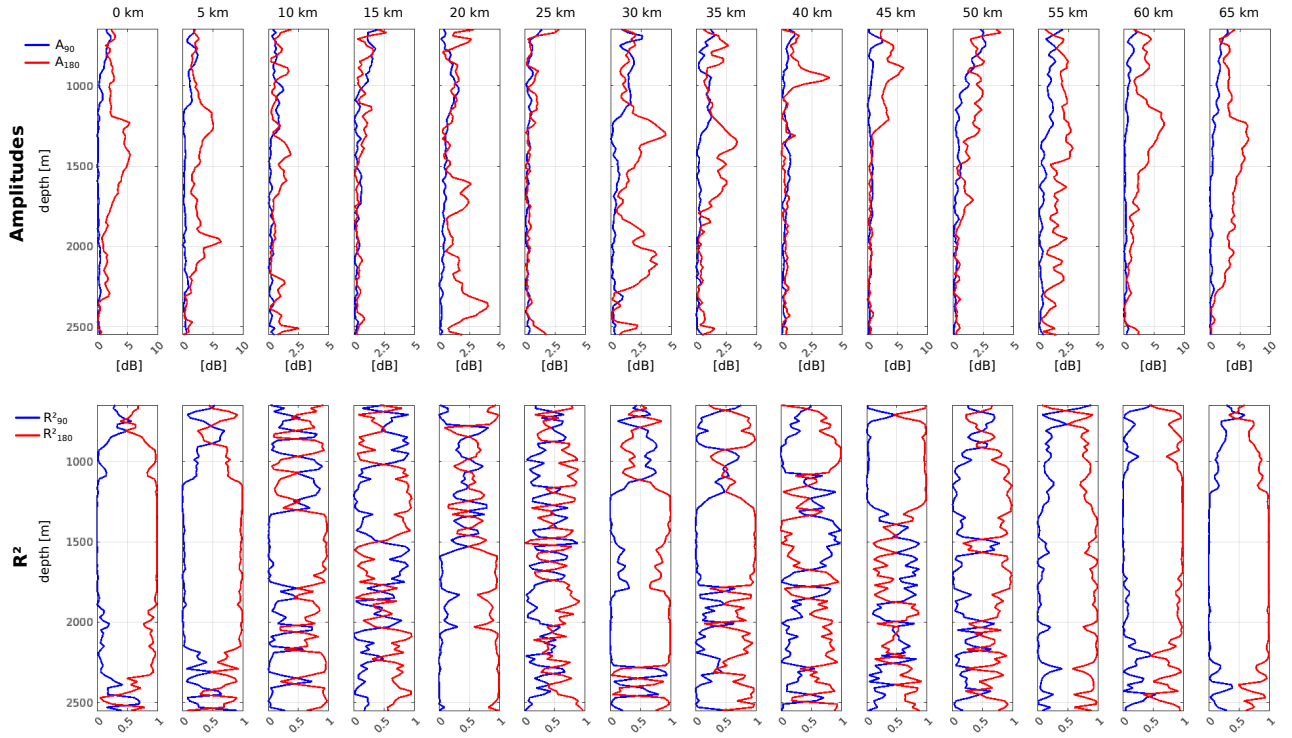

Fig. S11: mplitudes and goodness of fit for 90°- and 180°-periodic sine curve in profile '20220628'. Top panels show the amplitudes of birefringence (blue) and scattering (red) in dB at 5 km intervals along the profile, with start and driving direction indicated in Fig. S1. Bottom panels show the coefficient of determination (R^2), indicating the goodness of the fit, ranging from 0 to 1, for both curves.
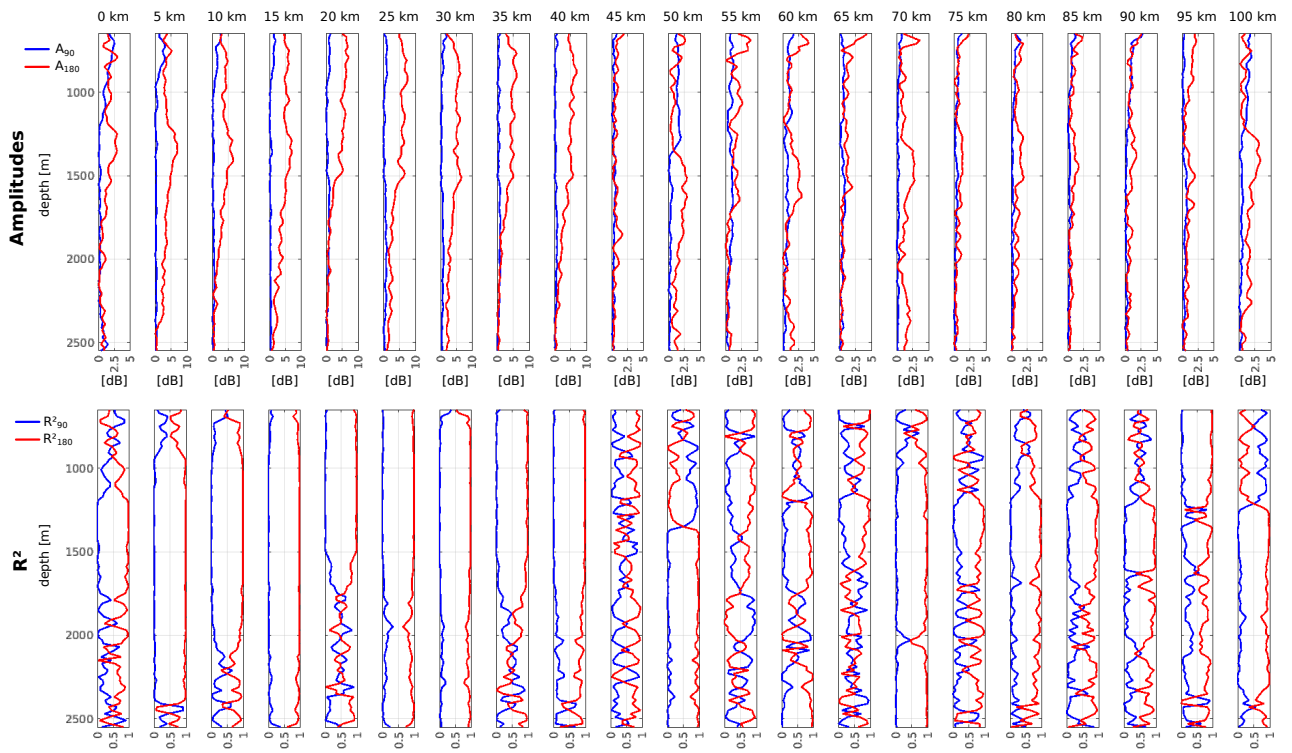
Fig. S12: Amplitudes and goodness of fit for 90°- and 180°-periodic sine curve in profile A (see Fig. 1). Top panels show the amplitudes of birefringence (blue) and scattering (red) in dB at 5 km intervals along the profile, with start and driving direction indicated in Fig. S1. Bottom panels show the coefficient of determination (R^2), indicating the goodness of the fit, ranging from 0 to 1, for both curves.
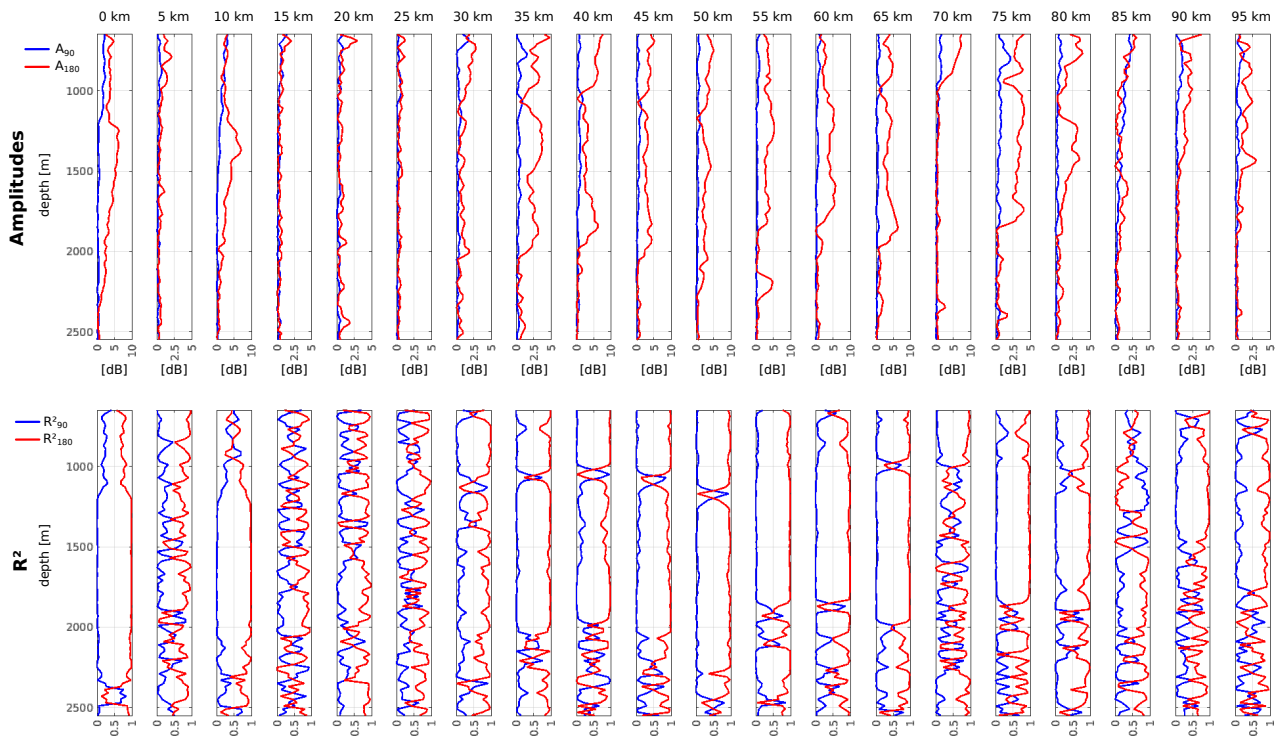
Fig. S13: Amplitudes and goodness of fit for 90°- and 180°-periodic sine curve in profile B (see Fig. 1). Top panels show the amplitudes of birefringence (blue) and scattering (red) in dB at 5 km intervals along the profile, with start and driving direction indicated in Fig. S1. Bottom panels show the coefficient of determination (R^2), indicating the goodness of the fit, ranging from 0 to 1, for both curves.